JOURNAL OF SOLID STATE CHEMISTRY **123,** 54–59 (1996)
ARTICLE NO. 0151

Hydrothermal Synthesis, Crystal Structure, and Magnetic Properties of $FeVO_4$-II

Yoshio Oka,* Takeshi Yao,† Naoichi Yamamoto,‡ Yutaka Ueda,§ Shuji Kawasaki,‖ Masaki Azuma,‖ and Mikio Takano‖

*Department of Natural Environment Sciences, Faculty of Integrated Human Studies; †Division of Energy and Hydrocarbon Chemistry, Graduate School of Engineering; and ‡Graduate School of Human and Environmental Studies, Kyoto University, Kyoto 606, Japan; §Institute for Solid State Physics, University of Tokyo, Tokyo 106, Japan; and ‖Institute for Chemical Research, Kyoto University, Uji, Kyoto 611, Japan

Received September 11, 1995; in revised form January 16, 1996; accepted January 17, 1996

$FeVO_4$-II, a metastable phase so far produced under high pressures, has been synthesized by a hydrothermal method from a solution of $VOCl_2$ and $FeCl_3$. $FeVO_4$-II crystallizes in the orthorhombic system: *Cmcm*, $a = 5.6284(7)$ Å, $b = 8.2724(7)$ Å, $c = 6.1118(6)$ Å, with $Z = 4$. The single-crystal structure refinements verified a $CrVO_4$-type structure and converged to $R/R_w = 0.035/0.029$ for 324 reflections with $I > 3\sigma(I)$. The structure consists of FeO_6 octahedra and VO_4 tetrahedra where edge-sharing FeO_6 octahedra form isolated FeO_4 chains running parallel to the *c* axis and the chains are joined by VO_4 tetrahedra. The temperature dependence of magnetic susceptibility featured by a broad maximum around 52 K suggests the predominance of one-dimensional antiferromagnetic interactions in the FeO_4 chains. A three-dimensional antiferromagnetic order is attained somewhere below 40 K yielding a hyperfine field of 483 KOe at 4.2 K observed in the Mössbauer spectrum.

INTRODUCTION

Iron (III) vanadate $FeVO_4$ exhibits four polymorphs designated as $FeVO_4$-I, II, III, and IV of which the type I is in a equilibrium state under the ambient condition (1). The structure of the triclinic $FeVO_4$-I was revealed by a single-crystal study to consist of two FeO_6 octahedra, one FeO_5 trigonal bipyramid, and three VO_4 tetrahedra where Fe–O polyhedra form a doubly bent chain (2). Other polymorphs were assumed from the powder X-ray diffraction data to have the orthorhombic $CrVO_4$ structure for $FeVO_4$-II, the orthorhombic α-PbO_2 for $FeVO_4$-III, and the monoclinic wolframite $NiWO_4$ for $FeVO_4$-IV (1,3,4); however, no structures of the phases have been fully characterized. The metastable phases of $FeVO_4$ are normally formed under high-pressure and high-temperature conditions. Muller and Joubert (1) reported that $FeVO_4$-III and IV were obtained directly by the high-pressure and high-temperature synthesis and $FeVO_4$-II emerged as an intermediate phase transformed from $FeVO_4$-III around 540°C with a narrow range of stability up to 570°C. Hotta *et al.* (5), on the other hand, constructed the pressure-product diagram of the $Fe_{1-x}V_xO_2$ system for $0 \leq x \leq 0.5$ at 800°C where $FeVO_4$ ($x = 0.5$) exhibited successive transformations I → II → III → IV with increasing pressures.

In the present study, we have empoyed a hydrothermal method and successfully obtained single crystals of the metastable polymorph $FeVO_4$-II. A single-crystal X-ray analysis has verified the $CrVO_4$-type structure and the measurements of magnetic susceptibility and Mössbauer effect revealed the occurrence of antiferromagnetic order.

EXPERIMENTAL

Sample Preparation

Starting materials used in the hydrothermal synthesis were aqueous solutions of $VOCl_2$ and $FeCl_3$ with V/Fe molar ratios of 0.5 to 1.0 where the concentration of $FeCl_3$ was fixed to 0.1 mol/liter. The solutions were sealed in Pyrex ampoules and treated hydrothermally at 280°C or 40 h. Orange black products were separated by filtration and washed thoroughly with distilled water. The crystalline phase of the product was identified by powder X-ray diffractometry to be $FeVO_4$-II (1). An Fe/V atomic ratio was determined by a energy dispersive X-ray analysis to be 0.99(1), which confirms the stoichiometric composition of $FeVO_4$. As shown in an SEM micrograph in Fig. 1, the products were single-crystalline granules with a particle size of 0.1 to 0.3 mm.

Magnetic Property Measurements

Magnetic susceptibility was measured by using a SQUID magnetometer under a magnetic field of 1000 G in a temperature range from 5 to 300 K. The Mössbauer effect was observed at 4.2 K, 77 K, and RT using $^{57}Co/Rh$ as a γ-ray source and pure Fe metal as a standard. As-synthesized granules were used in both measurements.

0022-4596/96 $18.00

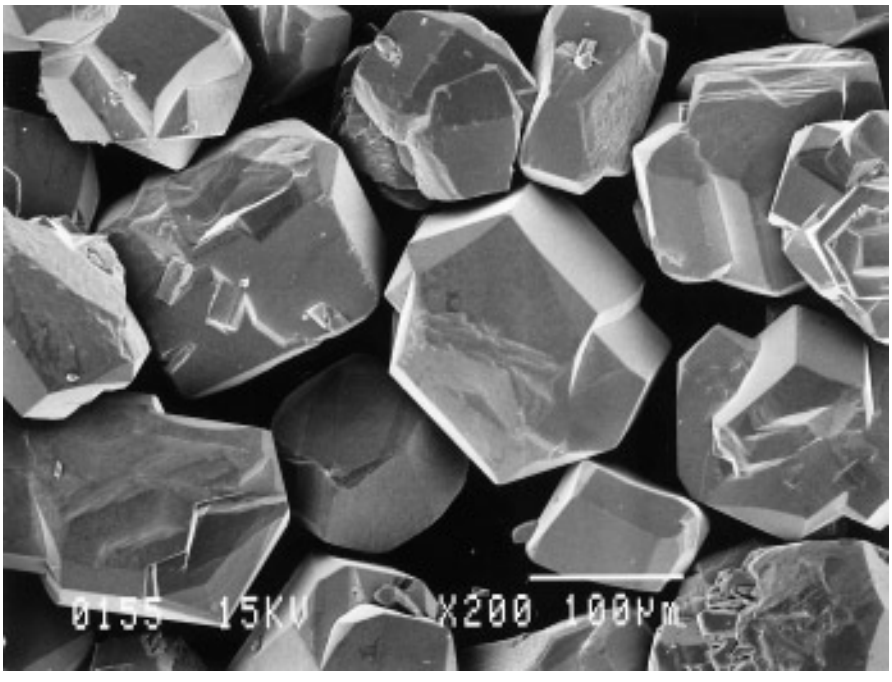

FIG. 1. Scanning electron micrograph of $FeVO_4$-II crystals.

Single-Crystal X-Ray Diffraction Study

Data collection was made on a single crystal of 0.15 × 0.15 × 0.05 mm in size using a Rigaku AFC-7R diffractometer with monochromated Mo$K\alpha$ radiation. The crystal system is orthorhombic and the lattice constants were determined from 22 reflections in a range $22.1° < 2\theta < 26.9°$ as $a = 5.6284(7)$ Å, $b = 8.2724(7)$ Å, and $c = 6.1118(6)$ Å. A unit cell volume of 284.57(5) Å^3 yielded $Z = 4$. Systematic extinction of $h + k = 2n + 1$ for hkl and $l = 2n + 1$ for $h0l$ gave space groups $Cmcm$ and $C2cm$ of which $Cmcm$ was chosen since the statistical treatment of intensity data indicated a centrosymmetric space group. Intensity data were collected by using the 2θ-ω scanning method up to $2\theta = 80°$. Standard reflections of 1 −3 0, 2 −4 −2, and 1 −1 2 were monitored every 150 reflection and no significant intensity deviation was detected. An empirical correction of absorption effect was made by the ψ scan method resulting in transmission factors ranging from 0.94 to 1.09. Finally 527 reflections with $I > 0$ were collected of which 324 reflections with $I > 3\sigma(I)$ were used in the structure analysis. According to the result of powder X-ray diffractometry (1), a $CrVO_4$- type structure was employed as an initial model. Atomic scattering factors for neutral atoms were taken from ''International Tables for X-ray Crystallography IV'' (6). The structure analysis calculations were performed by using the TEXSAN crystallographic software package (7). The structure model was successfully applied and the full-matrix least-square refinements converged to $R = 0.035$ and $R_w = 0.029$ for 22 parameters. The crystallogrpahic data and experimental parameters are listed in Table 1 and the atomic parameters and isotropic temperature factors in Table 2.

RESULTS

Hydrothermal Synthesis of $FeVO_4$-II

The hydrothermal system of $VOCl_2$–$FeCl_3$ produced the metastable phase of $FeVO_4$-II. The formation of $FeVO_4$-II

TABLE 1
Crystallographic Data and Experimental Parameters for $FeVO_4$-II

Chemical formula	$FeVO_4$
Space group	*Cmcm*
a (Å)	5.6284(7)
b (Å)	8.2724(7)
c (Å)	6.1118(2)
Z	4
D_c (g cm^{-3})	3.986
Crystal size (mm)	0.15 × 0.15 × 0.05
Radiation	Mo$K\alpha$
Scan technique	$2\theta - \omega$
Scan width, $\Delta\omega$ (°)	1.00 + 0.30 tan θ
$2\theta_{max}$ (°)	80
Range of measured hkl	$0 \le h \le 10$, $0 \le k \le 14$, $0 \le l \le 11$
No. of reflections ($I > 0$)	527
No. of reflections ($I > 3\sigma(I)$)	324
No. of variables	22
R	0.035
R_w	0.029

TABLE 2
Atomic Parameters and Isotropic Temperature Factors for $FeVO_4$-II

Atom	Position	x	y	z	B_{eq} (Å^2)
Fe	4*a*	0	0	0	0.54(3)
V	4*c*	0	0.3599(1)	0.25	0.43(3)
O(1)	8*f*	0	0.2413(4)	0.0324(5)	0.6(1)
O(2)	8*g*	0.2353(5)	−0.0199(4)	0.25	0.6(1)

TABLE 3
Bond Distances (Å) and Angles (°) for VO_4 Tetrahedron and FeO_6 Octahedron in $FeVO_4$-II

VO_4 tetrahedron			
V–O(1)^{i,ii}	1.652(3)	V–O(2)^{iii,iv}	1.792(3)
O(1)^{i}–V–O(1)^{ii}	107.2(2)	O(1)^{i}–V–O(2)^{iii}	109.24(7)
O(1)^{i}–V–O(2)^{iv}	109.24(7)	O(1)^{ii}–V–O(2)^{iii}	109.24(7)
O(1)^{ii}–V–O(2)^{iv}	109.24(7)	O(1)^{ii}–V–O(2)^{iv}	112.5(2)
FeO_6 octahedron			
Fe–O(1)^{i,v}	2.006(3)	Fe–O(2)^{i,v,vi,vii}	2.029(3)
O(1)^{i}–Fe–O(1)^{v}	180	O(1)^{i}–Fe–O(2)^{i}	90.4(1)
O(1)^{i}–Fe–O(2)^{v}	89.6(1)	O(1)^{i}–Fe–O(2)^{vi}	89.6(1)
O(1)^{i}–Fe–O(2)^{vii}	90.4(1)	O(1)^{v}–Fe–O(2)^{i}	89.6(1)
O(1)^{v}–Fe–O(2)^{v}	90.4(1)	O(1)^{v}–Fe–O(2)^{vi}	90.4(1)
O(1)^{v}–Fe–O(2)^{vii}	89.6(1)	O(2)^{i}–Fe–O(2)^{v}	98.5(1)
O(2)^{i}–Fe–O(2)^{vi}	180	O(2)^{i}–Fe–O(2)^{vii}	81.5(1)
O(2)^{v}–Fe–O(1)^{vi}	81.5(1)	O(2)^{v}–Fe–O(2)^{vii}	180
O(1)^{vi}–Fe–O(2)^{vii}	98.5(1)		

Symmetry code: (i) x, y, z; (ii) $x, y, \frac{1}{2} - z$; (iii) $\frac{1}{2} - x, \frac{1}{2} + y, z$; (iv) $x - \frac{1}{2}, \frac{1}{2} + y, z$; (v) $x, -y, -z$; (vi) $-x, -y, -z$; (vii) $-x, y, z$.

was also observed using $VO(OH)_2$ or V_2O_5 powders instead of $VOCl_2$ for a vanadium source and $Fe(NO_3)_3$ for an iron source. However, the by-product of α-Fe_2O_3 was present to some extent in all cases, where fortunately $FeVO_4$-II mostly appeared in a form of single-crystalline granules and was therefore easily separated from fine powders of α-Fe_2O_3. Among other $FeVO_4$ polymorphs, $FeVO_4$-I was formed together with $FeVO_4$-II and α-Fe_2O_3 in the hydrothermal system of V_2O_5–$FeCl_3$ but the phase was hardly separated from α-Fe_2O_3 because of the particle shape being fine powders. $FeVO_4$-III and IV have not been synthesized in present hydrothermal systems. In a differential thermal analysis (DTA) the hydrothermal $FeVO_4$-II was found to be converted into the equilibrium phase of $FeVO_4$-I above 400°C showing a broad endothermic DTA peak. The endothermic process may reflect a rise in entropy resulting from the volume expansion by 8% from $FeVO_4$-II to $FeVO_4$-I (1).

Crystal Structure of $FeVO_4$-II

Figure 2 depicts the structure of $FeVO_4$-II consisting of FeO_6 octahedra and VO_4 tetrahedra. Table 3 lists the bond distances and angles for the polyhedra, both of which appear little distorted. The structural feature of $FeVO_4$-II is that edge-shared FeO_6 octahedra form one-dimensional FeO_4 chains running along the c axis at (0, 0) and $(\frac{1}{2}, \frac{1}{2})$ in (x, y), where the Fe–Fe distance along the chain is 3.056 Å. As demonstrated by the polyhedral representation in Fig. 3, the chains are not directly connected with each other but are linked through VO_4 tetrahedra by sharing vertices, where the Fe–Fe distance between neighboring chains is 5.003 Å. The VO_4 tetrahedra also bridge intrachain FeO_6 octahedra by sharing vertices alternately from either side of the chain, which leads to a slight corrugation of the FeO_4 chain.

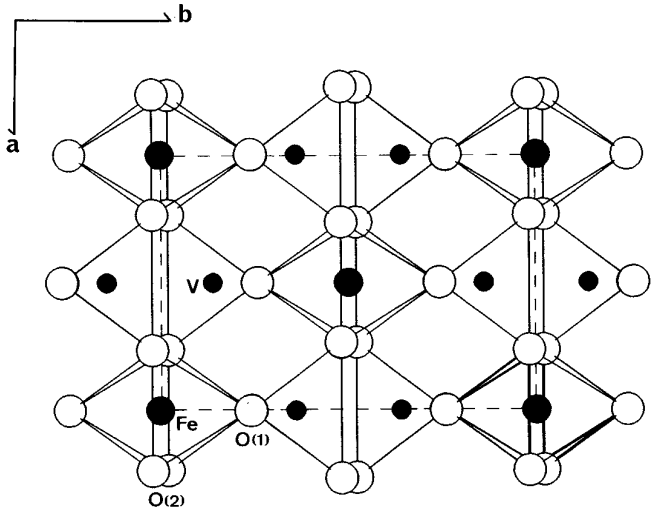

FIG. 2. Crystal structure of $FeVO_4$-II viewed along the c axis. A unit cell is indicated by broken lines.

Magnetic Properties of $FeVO_4$-II

Figure 4 shows the temperature dependence of magnetic susceptibility of $FeVO_4$-II. At temperatures above about 100 K it follows the Curie–Weiss law with a Weiss constant of $\Theta = -201$ K and an effective magnetic moment of 6.29 μ_B. The value of the effective moment is somewhat higher than the calculated value of 5.90 μ_B for a high-spin Fe^{3+} ion ($S = \frac{5}{2}$, $g = 2$). Below about 100 K the susceptibility curve starts to deviate from the Curie–Weiss plot toward a broad peak and 52 K. It should be also noticed that the susceptibility curve abruptly drops below 40 K, which, taking into account of the results of a Mössbauer study to be described below, is interpreted as the onset of antiferromagnetic order.

The Mössbauer spectra at RT, 77 K, and 4.2 K are shown in Fig. 5, and the fitting parameters are given in Table 4. Both at RT and 77 K a single kind of quadrupole, doublet was observed and the isomer shift relative to Fe metal is

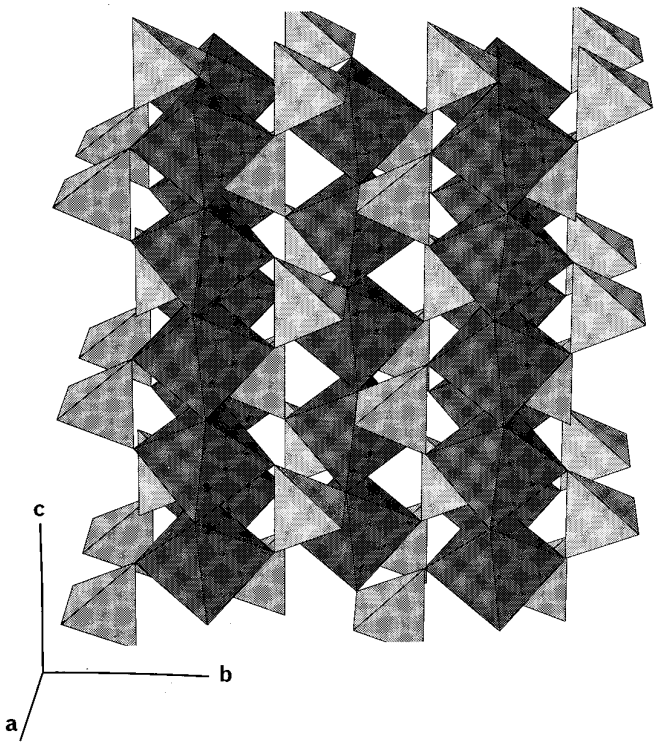

FIG. 3. Polyhedral representation of the $FeVO_4$-II structure consisting of FeO_6 octahedra and VO_4 tetrahedra.

typical of Fe^{3+} ions in oxides. The spectrum at 4.2 K exhibits a large magnetic hyperfine field of 483 kOe. These results are consistent with the susceptibility data in a sense that the Fe^{3+} ions are in a high-spin state and get magnetically ordered at about 40 K. To be noted here is the fact that the quadrupole doublet and the magnetic pattern are both anomalous with respect to the peak intensity: the low-energy peak of the quadrupole doublet is stronger than the high-energy peak, though the most common intensity ratio is 1 : 1 for a powdered sample, and, at the same time, the six-fingered magnetic pattern does not show the usual 3 : 2 : 1 ratio. We believe that these result from preferred orientation of the single-crystalline sample powder.

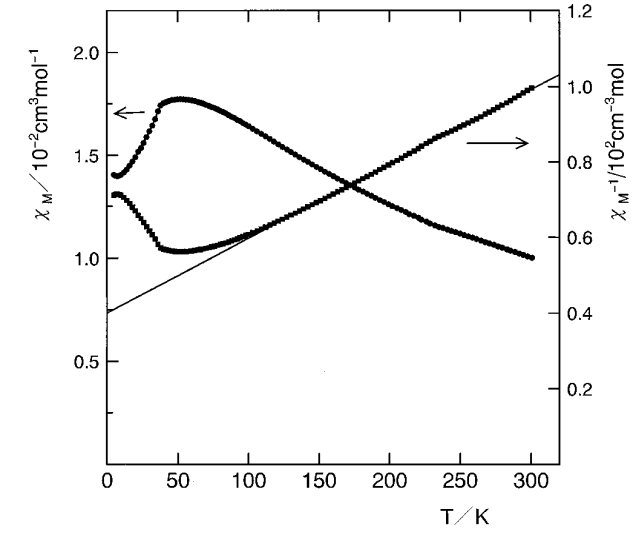

FIG. 4. Temperature dependence of the magnetic susceptibility and inverse susceptibility for $FeVO_4$-II.

DISCUSSION

This study presents a solution process of a hydrothermal method to produce metastable $FeVO_4$-II. The synthetic methods so far reported utilized high-pressure processes (1, 3–5). For example, Muller and Joubert (1) employed 800–1300°C and 20–80 kbar to prepare $FeVO_4$-III and IV and first found $FeVO_4$-II as a phase conversion product from $FeVO_4$-III. Later, Hotta *et al.* (5) prepared directly $FeVO_4$-II under 10–20 kbar at 800°C as well as $FeVO_4$-III and IV under higher pressures. An aqueous process was applied to the preparation of $FeVO_4$ by Touboul and Popot (8) who studied the synthesis of a series of orthovanadates RVO_4 (R = In, Fe, Cr, Al, Nd, Y). They, however, obtained amorphous hydrous phase of $FeVO_4$ from the V_2O_5–$Fe(NO_3)_3$ system treated in boiling water. This indicates that the hydrothermal process is indispensable to producing crystalline $FeVO_4$. Actually, for $(Cr_{0.5}Fe_{0.5})VO_4$ a $CrVO_4$-type compound was synthesized by the hydrothermal treatment at 350°C for 12 h (9). However, it was also reported that the trial to prepare $FeVO_4$-II by hydrothermal phase conversion from $FeVO_4$-I was unsuccessful (9). This suggests that crystalline $FeVO_4$ is formed in a direct precipitation process from aqueous vanadium and iron species.

There exist four polymorphs for $FeVO_4$, namely I, II, III, and IV. $FeVO_4$-II has been confirmed here to adopt the $CrVO_4$-type structure using single-crystal data as well as the triclinic $FeVO_4$-I (2). Taking it for granted that $FeVO_4$-III and IV have the orthorhombic α-PbO_2 and the monoclinic wolframite $NiWO_4$ structures, respectively, the polymorphs have different metal–oxygen environments: FeO_6 octahedra, FeO_5 trigonal bipyramids, and VO_4 tetrahedra in $FeVO_4$-I, FeO_6 octahedra and VO_4 tetrahedra in $FeVO_4$-II, and FeO_6 and VO_6 octahedra in $FeVO_4$-III and IV (1). The average coordination number becomes larger in order from I to IV indicating that the atomic packing becomes denser in this order. Actually, the volume per formula unit decreases as 78.2 $Å^3$ for I, 71.9 $Å^3$ for I, 61.3 $Å^3$ for III, and 60.4 $Å^3$ for IV (1).

The $CrVO_4$-type structure is reported for other orthovanadates MVO_4 for M = Cr (10), In (11), and Tl (12). The structure of $CrVO_4$ was first determined by Brandt (10) and later a full single-crystal X-ray analysis of the $CrVO_4$-type structure was made on $InVO_4$ by Touboul

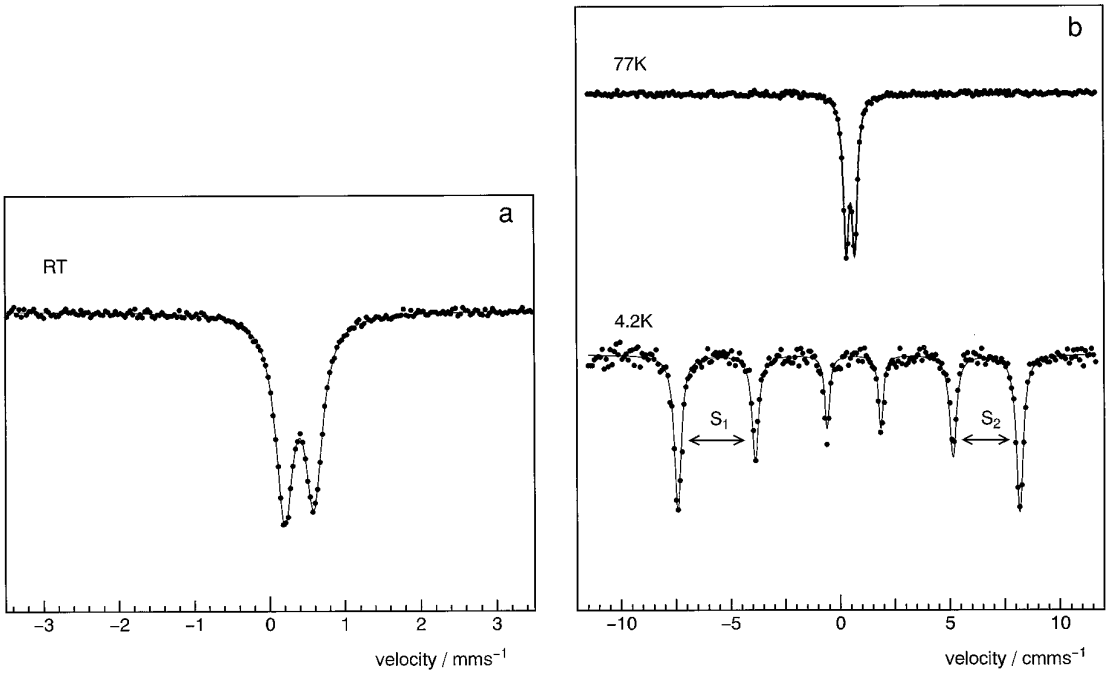

FIG. 5. Mössbauer spectra of $FeVO_4$-II: (a) RT, (b) 77 and 4.2 K.

and Tolédano (11). Table 5 lists the lattice parameters and unit cell volumes for the $CrVO_4$-type orthovanadates. The ionic radii of M^{3+} ions (13) range rather widely from 0.615 Å for Cr^{3+} to 0.886 Å for $T1^{3+}$ and as shown in Fig. 6 the lattice constants as well as the unit cell volume increase almost linearly with increasing ionic radius. For a smaller M^{3+} ion of $A1^{3+}$ $A1VO_4$ was suggested from powder X-ray diffraction data to adopt the $FeVO_4$-I structure instead of the $CrVO_4$ type (14), and hence $A1VO_4$ should have AlO_5, $A1O_6$, and VO_4 polyhedra. Yamaguchi *et al.* (15), however, claimed the existence of $A1O_6$ octahedra, $A1O_4$ tetrahedra, and VO_4 tetrahedra from an IR study. For large M^{3+} ions such as lanthanide metals, orthovanadates MVO_4 crystallize mostly in the zircon-type structure with MO_8 polyhedra joined by VO_4 tetrahedra (16). It is noted that $ScVO_4$ with an ionic radius of SC^{3+} being 0.745 Å adopts the zircon-type instead of the $CrVO_4$-type structure (16).

TABLE 4
Isomer Shift (IS) Quadrupole Splitting ($e^2qQ/2$) and Hyperfine Field (H_{hf}) for $FeVO_4$-II

T (K)	IS (mm s^{-1})	$e^2qQ/2$ (mm s^{-1})	H_{hf} (kOe)
RT	0.39	0.39	0
77	0.51	0.39	0
4.2	0.51	−0.26[a]	483

[a] $S_1 - S_2 = -0.255$ mm s^{-1} (see Fig. 5b).

The magnetic susceptibility curve of $FeVO_4$-II exhibiting a broad maximum below about 100 K seems to suggest one-dimensional antiferromagnetic behavior. Similar behavior was observed in $CrVO_4$ below 100 K and was discussed based on a one-dimensional model (17). The one-dimensional magnetic coupling of Fe^{3+} ions corresponds well to the structural feature of an isolated one-dimensional chain of FeO_6 octahedra along the c axis as shown in Fig. 3. However, a preliminary approach utilizing a modified Fisher model of a Heisenberg linear-chain antiferromagnet with $S = \frac{5}{2}$ (19), which was successfully applied to a Mn^{2+}

TABLE 5
Lattice Parameters (Å) and Unit Cell Volumes (Å^3) of $CrVO_4$-type Orthovanadates

	a	b	c	V	Ref.
$CrVO_4$	5.568	8.208	5.977	273.2	(10)
	5.589(0)	8.252(1)	5.993(1)	276.4	(17)
	5.5811(4)	8.2379(5)	5.9946(4)	275.6	(18)
$(Cr_{0.5}Fe_{0.5})VO_4$	5.6115(6)	8.2624(9)	6.0691(7)	281.2	(9)
$FeVO_4$	5.646(4)	8.303(5)	6.134(4)	287.6	(1)
	5.6284(7)	8.2724(7)	6.1118(6)	284.6	this work
$InVO_4$	5.765(4)	8.542(5)	6.592(4)	324.6	(11)
$T1VO_4$	5.839(3)	8.687(6)	6.800(4)	344.9	(12)

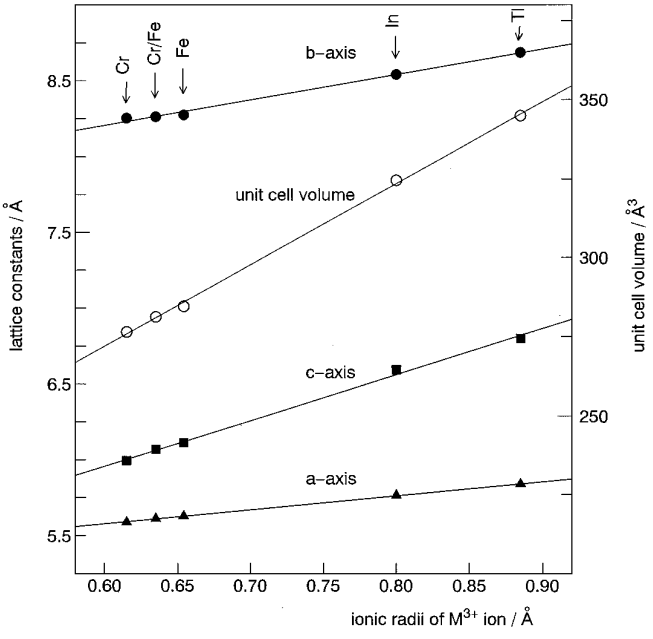

FIG. 6. Variations of lattice parameters and unit cell volumes with the ionic radii of M^{3+} ions for $CrVO_4$-type orthovanadates MVO_4 for M = Cr, Cr/Fe (an equimolar ratio), Fe, In, T1. An average ionic radius is adopted for M = Cr/Fe with an equimolar ratio.

system of $[(CH_4)_4N][MnCl_3]$ (20), was not successful, probably because inter-chain interactions are considerably strong. The inter-chain interactions lead to the three-dimensional antiferromagnetism somewhere below 40 K. The hyperfine field of 483 kOe at 4.2 K is comparable with that of 465 kOe or the triclinic $FeVO_4$-I having a Néel temperature of 22 K (2, 21).

ACKNOWLEDGMENT

The present work is supported by Grant-in-Aid for Scientific research for the Ministry of Education, Science, and Culture of Japan.

REFERENCES

1. J. Muller and J. C. Joubert, *J. Solid State Chem.* **14,** 8 (1975).
2. B. Robertson and E. Kostiner, *J. Solid State Chem.* **4,** 29 (1972).
3. A. P. Young and C. M. Schwartz, *Acta Crystallogr.* **15,** 1305 (1962).
4. F. Laves, *Acta Crystallogr.* **17,** 1476 (1964).
5. Y. Hotta, Y. Ueda, N. Nakayama, K. Kosuge, S. Kachi, M. Shimada, and M. Koizumi, *J. Solid State Chem.* **55,** 314 (1984).
6. "International Tables for X-ray Crystallography IV." Kynoch Press, Birmingham, UK, 1974.
7. "TEXSAN: Crystal Structure Analysis Package." Molecular Structure Corporation, 1992.
8. M. Touboul and A. Popot, *Rev. Chim. Minér.* **22,** 610 (1985).
9. J. P. Attfield, *J. Solid State Chem.* **67,** 58 (1987).
10. K. Brandt, *Arkiv. Kemi., Miner. Geol. A* **17,** 1 (1943).
11. M. Touboul and P. Tolédano, *Acta Crystallogr. Sect. B* **36,** 240 (1980).
12. M. Touboul and D. Ingrain, *J. Less-Common Met.* **71,** 55 (1980).
13. R. D. Shannon and C. T. Prewitt, *Acta Crystallogr. Sect. B* **25,** 925 (1969).
14. E. J. Baran and I. L. Botto, *Monatsh. Chem.* **108,** 311 (1977).
15. O. Yamaguchi, T. Uegaki, Y. Miyata, and K. Shimizu, *J. Am. Ceram. Soc.* **70,** C198 (1987).
16. B. C. Chakoumakos, M. M. Abraham, and L. A. Boatner, *J. Solid State Chem.* **109,** 197 (1994).
17. M. J. Isasi, R. Sáez-Puche, M. L. Veiga, C. Pico, and A. Jerez, *Mater. Res. Bull.* **23,** 595 (1988).
18. JCPDS 38-1376.
19. G. R. Wagner and S. A. Friedberg, *Phys. Lett.* **9,** 11 (1964).
20. R. Dingle, M. E. Lines, and S. L. Holt, *Phys. Rev.* **187,** 643 (1969).
21. L. M. Levinson and B. M. Wanklyn, *J. Solid State Chem.* **3,** 131 (1971).